Superradiance Steering, Switching, and Trapping in a Two-Dimensional Photonic Bandgap Structure

Igor V. Mel'nikov, Joseph W. Haus, *Fellow, IEEE,* and J. Stewart Aitchison*, Senior Member, IEEE*

Abstract - **We study the superradiant decay of an ensemble of inverted two-level atoms embedded into both a continuous dielectric and a 2D photonic crystal with lateral confinement of the radiation. The nonlinear superradiance pulse characteristics are calculated using a Green function based model. Specifically, we predict fast phase synchronization across the ensemble that builds up a distributed feedback structure responsible for the superradition anisotropy and directional switching. We show that the transfer of the optical excitation takes place along the Bragg planes and is manifested by strong energy localization.**

Index terms - **Superradiance, nanostructures, photonic crystals, quantum optics**

1. Introduction

Photonic crystals (PhCs) have been the subject of a growing number of studies [1-5], and there is a great deal of activity nowadays largely due to dramatic achievements in the fabrication of optical materials with periodically varied optical characteristics [6]. The PhC is a one-, two-, or three-dimensional structure with a periodically modulated dielectric function and whose period of modulation is on the order of the optical wavelength. The optical characteristics of PhCs have profound implications for light localization [7], quantum state generation [8], high efficiency microlasers [9], optical sensors [10, 11], and a wide range of photonic devices [12].

Recent advances in the fabrication of such low-dimensional, nanometer-scale, semiconductor structures, such as quantum wires and dots, promise to form a unit cell for a new generation of engineered photonic crystals that integrate electronic properties with optical characteristics. The realization and optimization of optical exciton transport, sub-shot noise generation, and lasing in photonic crystals require a detail understanding of both electromagnetic and quantum confinement processes. In this paper, we explore the population and polarization dynamics that is the excitation transport, inside both a 2D continuous medium and a rectangular structure of quantum emitters. Representation of the solution of the wave equation of the emission field through a corresponding Green function enables us to describe its spatiotemporal confinement by the set of coupled ordinary differential equations, which can be solved by standard numerical methods.

Manuscript received November 8, 2005. This work was supported in parts by Natural Science and Engineering Research Council of Canada, Photonics Research Ontario, and Max-Planck-Gesellschaft.

I.V. Mel'nikov is now with Max-Planck-Institut für Physik Komplexer Systeme, Nöthnitzer Str. 38, 01187 Dresden, Germany and High Q Laboratories, Inc., 36 Howe Ave., Hamilton, Ontario, Canada L9A 1W7; he is on leave from A. M. Prokhorov General Physics Institute RAS, Moscow 119991, Russian Federation (corresponding author, phone: (905) 385-4519, fax: (416) 971-3020, e-mail: ivm@highqlabs.com).

J. W. Haus is with the Electro-Optics Program, School of Engineering, University of Dayton, 300 College Park, Dayton, Ohio 45469 - 0245

J. S. Aitchison is with the E. S. Rogers Sr. Department of Electrical and Computer Engineering, University of Toronto, 10 King's College Road, Toronto, Ontario, Canada M5S 3G4

This paper is organized as follows. In Section 2, we give a highlight of the Green function-based approach and derive an evolution equation for Bloch angles. Then, in Sec. 3, we analyze the superradiance in a localized system and discuss our approximations. In Section 4, we numerically obtain and discuss the superradiance pattern emerging from a pencil-like sample. Section 5 analyzes the structure of the excitation decay of the single atom embedded into a 2D photonic crystal. Finally, in Sec. 6, the results are summarized and applications are discussed.

2. The Model – Inhomogeneous Superradiance Field and Resonant Current

Consider a set of 2D emitters that is represented by a set of parallel wires filled with material that can be modeled as two-level atoms, which, in turn, can be described by the two Bloch angles, θ and φ. These angles are connected to the eigenfunctions $\psi_{\pm}$ and their phases $\varphi_{\pm}$ of the Hamiltonian of an isolated two-level atom in the following standard form [13]

$$\begin{aligned} &\left|\theta,\varphi_{\pm}\right\rangle \equiv \cos\frac{\theta}{2}\cdot e^{i\varphi_{+}}\left|\psi_{+}\right\rangle + \sin\frac{\theta}{2}\cdot e^{i\varphi_{-}}\left|\psi_{-}\right\rangle, \\ &\left|\psi_{+}\right\rangle = \begin{pmatrix}1\\0\end{pmatrix}, \quad \left|\psi_{-}\right\rangle = \begin{pmatrix}0\\1\end{pmatrix}. \end{aligned} \tag{1}$$

Upon the action of a complex external field, $E(x,y,t)$, the response of the single two-level emitter obeys the following equation [14]:

$$\begin{aligned} &\frac{1}{\cos\theta}\frac{d}{dt}\left(\sin\theta\, e^{i\varphi}\right) = \frac{2i\mu E(x,y,t)}{\hbar}\exp(i\omega_0 t), \\ &\varphi \equiv \varphi_{+} - \varphi_{-}, \end{aligned} \tag{2}$$

where μ is the electric dipole moment of the resonant transition, and $\hbar$ is the Planck constant.

The electromagnetic field in our model is treated classically; assume that the charge density is equal to zero, there is no damping, non-resonant losses, and nonlinearity of the host matrix. Then the Maxwell wave equation becomes

$$\left(\frac{\partial^2}{\partial x^2} + \frac{\partial^2}{\partial y^2} - \frac{1}{c^2}\frac{\partial^2}{\partial t^2}\right)E(x,y,t) = \frac{4\pi}{c^2}\frac{\partial J(x,y,t)}{\partial t}, \tag{3}$$

where x and y are the spatial coordinates, $J(x,y,t)$ is the current density that is perpendicular to the (x-y) plane. Bearing in mind the resonant nature of the spontaneous decay, we may introduce slow amplitude of the field $\mathcal{E}(r,t)$ and current $j_0(r,t)$ as

$$\begin{aligned} &\begin{pmatrix}E(r,t)\\J(r,t)\end{pmatrix} = \begin{pmatrix}\mathcal{E}(r,t)\\j_0(r,t)\end{pmatrix}\exp(-i\omega_0 t), \quad \frac{d}{dt}\begin{pmatrix}E(r,t)\\J(r,t)\end{pmatrix} << \omega_0\begin{pmatrix}\mathcal{E}(r,t)\\j_0(r,t)\end{pmatrix}, \\ &r = \sqrt{x^2+y^2}. \end{aligned} \tag{4}$$

Then Eq. (2) for the Bloch angles can be re-written as

$$\frac{1}{\cos\theta}\frac{d}{dt}\left(\sin\theta\, e^{i\varphi}\right) = \frac{2i\mu\mathcal{E}(r,t)}{\hbar}, \tag{5}$$

and in the 2D discrete dielectric medium, the slow amplitude $\mathcal{E}(r,t)$ that satisfies Maxwell equation (3) can be written as a function of the current density $j_0(r_m, t)$ in the following form:

$$\mathcal{E}(r,t) = -\frac{\pi k_0}{c}\sum_m H_0^{(1)}(k_0|\vec{r}-\vec{r}_m|)j_0(\vec{r}_m,t), \tag{6}$$

here $H_0^{(1)}$ is the Hankel function of the first kind, representing a Green function for outgoing waves, or retarded solutions of Maxwell's equations, k_0 is the wave vector, r_m is the position of the m^{th} emitter, and $j_0(r_m, t)$ is the amplitude of the m^{th} emitter current, which is proportional to the polarization of the two-level atom at the m^{th} site $p_m \equiv \sin\theta_m \cdot e^{i\varphi_m}$ and is written as:

$$j_0\left(\vec{r}_m,t\right) = S\mu\frac{\partial p_m}{\partial t}, \tag{7}$$

with S being the number of quantum emitters per unit length of the wire and we neglect a retardation effect in slow amplitudes; that is, we neglect the stimulated emission processes and thus consider the case of pure superradiative decay. Note that since $H_0^{(1)}(0) = -i\infty$, Eqs. (5) and (6) exclude self-action effects. In order to define the self-action correctly we use of Dirac method [15] that is based on an advanced solution for the wave equation:

$$\mathcal{E}_{adv}(r,t) = \frac{\pi k_0}{c}H_0^{(2)}(k_0 r)j_0(t), \tag{8}$$

where $H_0^{(2)}$ is the Hankel function of the second kind, and r is the distance from the source to the observation point. Following Dirac [10], the self-action field can be defined as follows:

$$\mathcal{E}'(t) = \lim_{r\to 0}\frac{\left[\mathcal{E}(r,t)-\mathcal{E}_{adv}(r,t)\right]}{2} = -\frac{\pi k_0}{c}j_0(t), \tag{9}$$

where we use the property of Hankel functions $H_0^{(1)}(x) - H_0^{(2)}(x) = 2J_0(x)$. In this result $J_0(x)$ is a Bessel function of the first kind and $J_0(0)=1$. Summarizing over Eqs. (5)-(9) we have the following set of complex equations:

$$\begin{aligned}&\frac{1}{\cos\theta_m}\cdot\frac{d}{d\tau}\left(\sin\theta_m\cdot e^{i\varphi_m}\right)+\sum_{n\neq m}H_0^{(1)}(k_0|r_m-r_n|)\cdot\sin\theta_n\cdot e^{i\varphi_n}\\&+\sin\theta_m\cdot e^{i\varphi_m}=0,\end{aligned} \tag{10}$$

that describe the spatio-temporal evolution of a 2D array of two-level emitters. The summation is over all emitters including the self-reaction. Note that in Eq. (7) we introduced a time normalization, $\tau \equiv (\pi\mu^2 k_0^2 S/\hbar)t$, and that at $m = n$ the Hankel function was replaced by unity. Radiation is confined to the interaction between dipoles on the rectangular lattice.

We must also take into account the quantum fluctuations that initiate the spontaneous decay, by including the term

$$\frac{8}{3\lambda S}\cdot\left[\tan\left(\frac{\theta_m}{2}\right)-\frac{\sin\theta_m}{2}\right]e^{i\varphi_m}, \tag{11}$$

into the right-hand side of Eq. (10). Note this contains a phase component so that rewriting Eqs. (10) and (11) in the form of the $2N$ real equations, with N being the total number of separate wires in the lattice, keeps it in a term that describes the evolution of θ_m. It is also worth noticing that setting the fluctuating field (11) equal to the regular field (10) yields the initial value of $\theta_m(0)$ whereas the initial phase $\varphi_m(0)$ is chosen to be an independent random function for all m in order to provide a non-correlated initial state of the array.

We conclude this Section with a note that the evolution equation (10) can be easily transformed for the case of a 2D continuous medium:

$$\left(\frac{\partial^2}{\partial x^2}+\frac{\partial^2}{\partial y^2}+k_0^2\right)\left[\frac{1}{\cos\theta}\frac{\partial}{\partial\tau}\left(\sin\theta\cdot e^{i\varphi}\right)\right]+4ik_0^2\sin\theta\cdot e^{i\varphi}=0, \tag{12}$$

which we shall exploit below in our modeling of the superradiance decay.

3. Spontaneous Decay in a Localized System

The set of equations (10), (11) can be studied analytically within the approximation of a localized system which linear size is much smaller than the resonant wavelength, $R \ll \lambda_0$. Let us now introduce the population inversion W_m and corresponding resonant polarization P_m of the m-th emitter as

$$W_m \equiv -\cos\theta_m, \quad P_m \equiv \sin\theta_m e^{i\varphi_m}, \tag{13}$$

and rewrite Eq. (10) in the form that does not depend on the sample dimensionality:

$$\begin{aligned}\frac{dP_m}{d\tau} &= W_m\sum_k G_{mk}P_k,\\ \frac{dW_m}{d\tau} &= -\mathrm{Re}\left[P_m^*\sum_k G_{mk}P_k\right].\end{aligned} \tag{14}$$

Here G_{mk} is the element of the matrix that determines interaction between separate emitters. It is given by the Green function for outgoing waves (see Eq. (6)) which can be substituted with its asymptotic in our case of the nanostructure $R \ll \lambda_0$:

$$G_{mk} \approx 1+\frac{2i}{\pi}\ln\left(k_0\left|\vec{r}_n-\vec{r}_k\right|\right). \tag{15}$$

The major quantity that characterizes the coherence in the localized system is a Bloch vector $\hat{S}$ whose components are defined as follows:

$$\hat{S} \equiv \left\{\mathrm{Re}\sum_m P_m, \mathrm{Im}\sum_m P_m, \sum_m W_m\right\}. \tag{16}$$

For this parameter, Eqs. (14) provide the following form

$$\frac{d}{d\tau}\left|\hat{S}\right|^2 = 2\sum_{m,n,k}\mathrm{Im}\,G_{mn}\left[W_n\,\mathrm{Im}\left(P_m^*P_k\right)+W_k\,\mathrm{Im}\left(P_m^*P_n\right)\right]. \tag{17}$$

Since Im$G_{mn} \neq 0$ (furthermore, Im $G_{mn} \to \infty$, see Eq. (15)), the Bloch vector is not conserved in a 2D case contrary to a 1D medium [16-19], and so the superradiance is not that evident to happen in such media. In the simplest case of only two inverted emitters, the analysis based on Eq. (17) demonstrates that the vector $\hat{S}$ oscillates around some average value with amplitude $\sim |\hat{s}_1 - \hat{s}_2|^2$ and the phases of the emitters are held locked (in other words, the coherence is maintained) provided $|\hat{s}_1 - \hat{s}_2| \ll 1$. At the same time, the frequency of the superradiance also experiences changes $\Delta\omega \sim$ Im G_{mn}.

It seems to be a normal practice to facilitate analysis and approach the solution of the superradiance spatio-temporal relaxation by assuming $R \ll c\tau_c$ or, in other words, that the decay is going on homogeneously along the sample. Besides, this requires the constant value of the phase φ for all emitters throughout the decay. In our previous publications we have shown these requirements are not satisfied even at $R \approx \lambda/2 \ll c\tau_c$ [14, 20, 21]. We are going to see in the next Section, the assumption of the inhomogeneous nature of the decay along with a denial of the constant phase approximation are capable of bringing in considerable modification of the superradiance in though pencil-like, nonetheless 2D, samples.

4. Superradiance in a Pencil-like Sample

Fig. 1 presents the numerical solution for the problem of superradiance relaxation of the 2D continuous sample with length $L = 3\lambda$ and width $b = 0.6\lambda$. The sample is supposed to be excited by a resonant coherent pulse that propagates along the longitudinal axis of the sample. For the sake of simplicity, quantum fluctuations of the dipole moment and radiation field are neglected and the initial Bloch angle is chosen to be same throughout the whole sample and equal to $\theta_0 = 0.1$. Since it is defined by the condition $I_s \sim I_r$ (that is, setting r.h.s. of Eq. (10) equal to Eq. (11)) and so is bound to the emitter density $\theta_0 \approx (\rho\lambda^2 L)^{-1/2}$, this gives the estimate for the density $\rho\lambda^3 \approx 100$. It is worth noticing here that the Fresnel number is equal to $F = b^2/(\lambda L) = 0.12 \ll 1$ and so an 1D approximation is not justified for this sample.

It is seen a distinct anisotropy of the superradiance dynamics. That is, assume a homogeneous density of the inversion population and continuous phase of the emitter current, $\varphi(x,y,t) = k_0 x$, across the sample; these are typical for the superradiance media mentioned in the Introduction. Then the supperradiance pattern of the 2D sample can be approximated with

$$I(\Phi,t) \simeq \frac{\sin^2\left[\frac{1}{2}k_0 L\left(1-\cos\Phi\right)\right]}{k_0^{\,2}L^2\left(1-\cos\Phi\right)^2}\,\frac{\sin^2\left(\frac{1}{2}k_0 b\sin\Phi\right)}{k_0^{\,2}b^2\sin^2\Phi}\,\mathrm{sech}^2\left(\frac{t-t_0}{2\tau_c}\right). \qquad (18)$$

This quantity can be interpreted as an interference add-up of all the emitters at the angle Φ counted from the longitudinal axis of the sample. The results of the nonlinear model which are presented in Fig. 1, show the location and shape of the side lobes to deviate from those provided by the estimate above. The most striking of these discrepancies is the considerable time delay experienced by the intensity to reach up its maximum at the off-axis direction. The ratio of the side lobe maximum intensity to that in the main maximum also contrasts the prediction of Eq. (18); that is, it gives us $I_1/I_0 \approx 0.05$ whereas Fig. 1 defines $I_1/I_0 \approx 0.17$.

These features remain valid for longer samples which are tempting to call a pencil-like one what is not physically correct. Fig. 2 shows both the temporal evolution of the superradiance (a) and its angular variation (b) for the sample with $L = 50\lambda$ and width $b = 1.75\lambda$. One of these retained is the eruption of the most powerful pulse into the forward direction whereas the much less intense side lobe pulses are generated with considerable time delay. Apart of these, our modeling also displays the self-organization of the periodic feedback structure along the sample axis in the early stage of the decay. Its period is equal to $\lambda/2$ and underlying physics has already been published elsewhere [14, 20]; this is why we do not show it here.

The appearance of this structure is important, however, for understanding the superradiance behavior of another sample which has $L = 25\lambda$, $b = 1.75\lambda$, and $\theta_0 = 5\bullet10^{-3}$; the later implies $\rho\lambda^3 \approx 10^4$ (see Fig. 3). In this sample, the main pulse is observed in the direction backward to the propagation of the pump

pulse. The forward-emitted pulse is substantially delayed and is not so intense. This result of the energy emission in the backward propagating mode is due to the two-wave coupling mediated by the self-organizing feedback that manifests itself as a quasi-1D grating with period $\lambda/2$ imprinted into the inversion profile at the early, linear stage of the decay.

In all these examples above, the initial phase $\varphi(x,y,t = 0)$ is assumed to be forced by the external coherent pump. In the case of its stochastic distribution, our analysis shows the emitter phase locking to take place on the time scale shorter than the relaxation due to a weak regular wave. This wave propagates from the sample center toward its boundaries, experiences the maximum gain along the longitudinal axis, and synchronizes the individual phases $\varphi(x,t) \approx k_0 x$. Therefore, the system spontaneously, though via a regular mean, locks itself up in the state with the coherent phase and generates the superradiance pulse with features given.

5. Spontaneous Emission Steering and Trapping

Figure 4 captures screening-and-steering scenario of spontaneous decay in 2D photonic crystal obtained by numerical integration of Eq. (10). It illustrates what happens when a single inverted emitter is located inside a 2D PhC composed of 10 x 10 array of identical emitters all of which are in the ground state, and where the size of the rectangular cell is λ x $\lambda/4$. A pronounced anisotropy in the outgoing emission is clearly observed, which occurs as a result of the different periodicities along x and y axes of the grating. That is, the Bragg planes cause screening of the spontaneous emission and steer it along the direction of the Bragg diffraction. At the same time, the excitation transfer is tied to the Bragg plane where the inverted emitter is located. Notice the partial recurrence phenomenon for the central dipole excitation; the population inversion of the central initially emitter obeys a damped oscillating function, but population from neighboring dipoles is redistributed to the central dipole causing the population to revive. This is due to the following dependence of the argument in the function of $H_0^{(1)}(ik_0|r_m - r_n|)$. That is, this happens owing to the interference and is not caused by the retardation that comes into action at much larger scales. The interference also affects the angle distribution of the outgoing emission by means of its damping in the direction where the diffraction condition is not satisfied. The emission illustrated in Fig. 5 was calculated using Eq. (6) for the field radiation pattern. There is a forward- and backward-anisotropy in Fig. 5 which is due to the choice of initial conditions for the central excitation.

These observations can be qualitatively explained on the basis of the conservation of the total Bloch angle pertinent to a Bragg grating. That is, the excitation transport in photonic crystals can be obtained by examining the behavior of the single emitter near the complete inversion state for a time scale larger than the phase locking time [14]. Assume that this inverted quantum emitter, atom or exciton, is embedded in a 1-D Bragg grating. The rest of N-1 quantum emitters are assumed to be in the ground state. Then the kinetic equation for the Bloch angle θ (10) can be rewritten in a mean-field sense as follows ($\theta_m = \pi + \theta - \theta_0$ for all m):

$$\frac{d\theta}{dt} = -\sin\theta - (N-1)\sin(\theta - \theta_0), \tag{12}$$

where θ_0 is the starting value of the Bloch angle of the excited emitter [14]. As readily seen from Eq. (11), in the early stage of the decay its rate is equal to the decay rate of an isolated emitter, and there is no influence from the grating provided by a periodic chain of emitters. However, at the time scales longer than the cooperation time τ_c, when $t \geq \tau_c = 1/N$ the excitation radiation terminates, and the angle θ takes the equilibrium value of $\theta_e \approx \theta_0 - \sin\theta_0 / N$. That is, the energy drops off as $\mathrm{E} \approx \sin^2\theta_0 / 2N$ and is followed by a freezing up the state of the excitation of the emitter. Correspondingly, the emitters in the grating which are initially in the ground state acquire the excitation of $\sin\theta_0 / N$, and a standing optical wave arises along the grating such that its nodes coincide with the emitters. The energy of the final state practically equals to the initial excitation that is the energy losses which are proportional to N^{-1}. Therefore,

the near-resonant grating is capable of screening the excitation in the directions corresponding to the Bragg diffraction. This can result in strong directionality in the spontaneous emission decay that may be useful for light steering in a multidimensional PhC.

6. Conclusions

In conclusion, we have presented a theoretical model and numerical results describing the spontaneous decay of optical excitation in a photonic crystal. It is shown that the transfer of the optical excitation goes along the longitudinal axis of the sample or, in the case of discrete photonic structure, along Bragg planes and is accomplished by strong energy localization. In particular, we have shown the superradiance pulse may be generated in the backward direction, relative to the pump pulse. In addition, it is observed the formation of the quasi-1D inversion pattern with the period of $\lambda/2$ that triggers the superradiance up. These results are obtained for the pencil-like samples, where the length considerably exceeds the width and where it is so tempting to represent the superradiance field in the form of superposition of 1D forward- and backward-propagating waves. We believe that our results may be useful for such closely related fields as nonlinear optical dynamics of quantum dot arrays and 2D PhC lasers. The more broad and diverse range of phenomena of general physical interest can also be exploited, this includes moving Bose-Einstein condensate, Josephson superlattice dynamics, nanomagnetic spectroscopy, and black hole evolution.

References

1. E. M. Purcell, "Spontaneous emission probabilities at radio frequencies," Phys. Rev. **69,** 681 (1946).
2. V. P. Bykov, "Spontaneous emission in a periodic structure," *Sov. Phys. JETP* **35,** 269-273 (1972); "Spontaneous emission from a medium with a band spectrum," *Sov. J. Quant. Electron*. **4,** 861-871 (1975).
3. E. Yablonovitch, "Inhibited spontaneous emission in solid-state physics and electronics," *Phys. Rev. Lett*. **58,** 2059-2062 (1987).
4. S. John, "Strong localization of photons in certain disordered dielectric superlattices," *Phys. Rev. Lett*. **58,** 2486-2489 (1987).
5. K. Ohtaka, "Energy-band of photons and low-energy photon diffraction," *Phys. Rev*. B **19**, 5057 - 5067 (1979).
6. M. Bertolotti, C.M. Bowden and C. Sibilia, eds., "*Nanoscale Linear and Nonlinear Optics*," (AIP, NY, 2000).
7. Y. A. Vlasov, M. A. Kaliteevski, and V. V. Nikolaev, "Different regimes of light localization in a disordered photonic crystal," *Phys. Rev.* B **60,** 1555-1562 (1999).
8. M. Woldeyohannes and S. John, "Coherent control of spontaneous emission near a photonic band edge: A qubit for quantum computation," *Phys. Rev*. **A 60,** 5046-5068 (1999).
9. M. Fujita and T. Baba, "Microgear laser," *Appl. Phys. Lett.* **80**, 2051-2053 (2002).
10. J. Dorvee and M. J. Sailor, "A low-power sensor for volatile organic compounds based on porous silicon photonic crystals," *Phys. Stat. Solid. A – Appl. Mater. Sci.* **202**, 1619-1623 (2005).
11. W. C. L. Hopman, P. Pottier, D. Yudistira *et al.,* "Quasi-one-dimensional photonic crystal as a compact building-block for refractometric optical sensors," IEEE Journ. Select. Top. Quant. Electron. **11,** 11-16 (2005).
12. See, e.g., the *Photonic Band-Gap Bibliography*, H. Everitt, and E. Yablonovitch, eds., at http://www.pbglink.com.
13. R. H. Dicke, "Coherence in spontaneous radiation processes," *Phys. Rev.* **93,** 99 - 110 (1954).
14. I. V. Mel'nikov, "Asymmetry of operation and energy trapping in a superradiant laser," *Phys. Rev. Lett.* **77,** 842 (1996).
15. P. A. M. Dirac, "Classical theory of radiating electrons," *Proc. Roy. Soc. London* **A 167,** 148 - 169 (1938).
16. S. Haas, T. Strouken, M. Hübner *et al.,* "Intensity dependence of superradiant emission from radiatively coupled excitons in multiple-quantum-well Bragg structures," *Phys. Rev.* **B 57,** 14860-14868 (1998).
17. K. Sakoda and J. W. Haus, "Superfluorescence in photonic crystals with pencil-like excitation," *Phys. Rev*. **A 68**, Art. No. 053809 (2003).
18. C. Sibilia, M. Centini, K. Sakoda *et al.,* "Coherent emission in one-dimensional photonic bandgap material," *J. Opt. A: Pure Appl. Opt*. **7,** S198-S206 (2005).
19. J. P. Clemens, L. Horvath, B. C. Sanders, and H. J. Carmichael, "Shot-to-shot fluctuations in the directed superradiant emission from extended atomic samples," *J. Opt. B: Quant. Semiclass. Opt*. **6,** S736-S741 (2004).
20. I.V.Mel'nikov, "Symmetry break-up in distributed coupling of counterpropagating waves in a superradiant laser," *JETP Lett*. **63,** 150-154 (1996); "Dynamic coupling and instability in a resonant superfluorescence," *Laser Physics* **5,** 797-800 (1995).
21. I.V. Mel'nikov, J.S. Aitchison, and J.W. Haus , "Spontaneous emission trapping and steering in a two-dimensional photonic bandgap structure," Optics Commun. **244**, 279-283 (2005).

FIGURE CAPTIONS

Fig. 1 Snapshots of the superradiance pattern for the sample with size 3λ x 0.6λ; the angle Φ is counted from the longitudinal axis of the sample that is the pump pulse propagation; time is given in the units of the coherence time.

Fig. 2 Superradiance decay of the pencil-like sample with size 50λ x 1.75λ: temporal evolution of the superradiance intensity at different angles (*a*); snapshot of the superradiance pattern in the vicinity of the central maximum, ring structure is clearly seen (*b*).

Fig. 3 Direction switching of the superradiance decay of the pencil-like sample with size 25λ x 1.75λ: temporal evolution of the superradiance intensity at different angles (*a*); snapshots of the superradiance pattern in the forward (*b*) and reverse direction (*c*).

Fig. 4 Spontaneous decay of a single inverted two-level atom inside 2D photonic crystal with unit cell size λ x $\lambda/4$; the snapshots of the inversion profile are given for the six consecutive moments of time (see the insets), in turn, normalized to the coherence time.

Fig. 5 Angular distribution of the spontaneous emission from 2D photonic crystal with unit cell size λ x $\lambda/4$ at T = 3.5; the angle orientation is given on the first of Figs. 4.

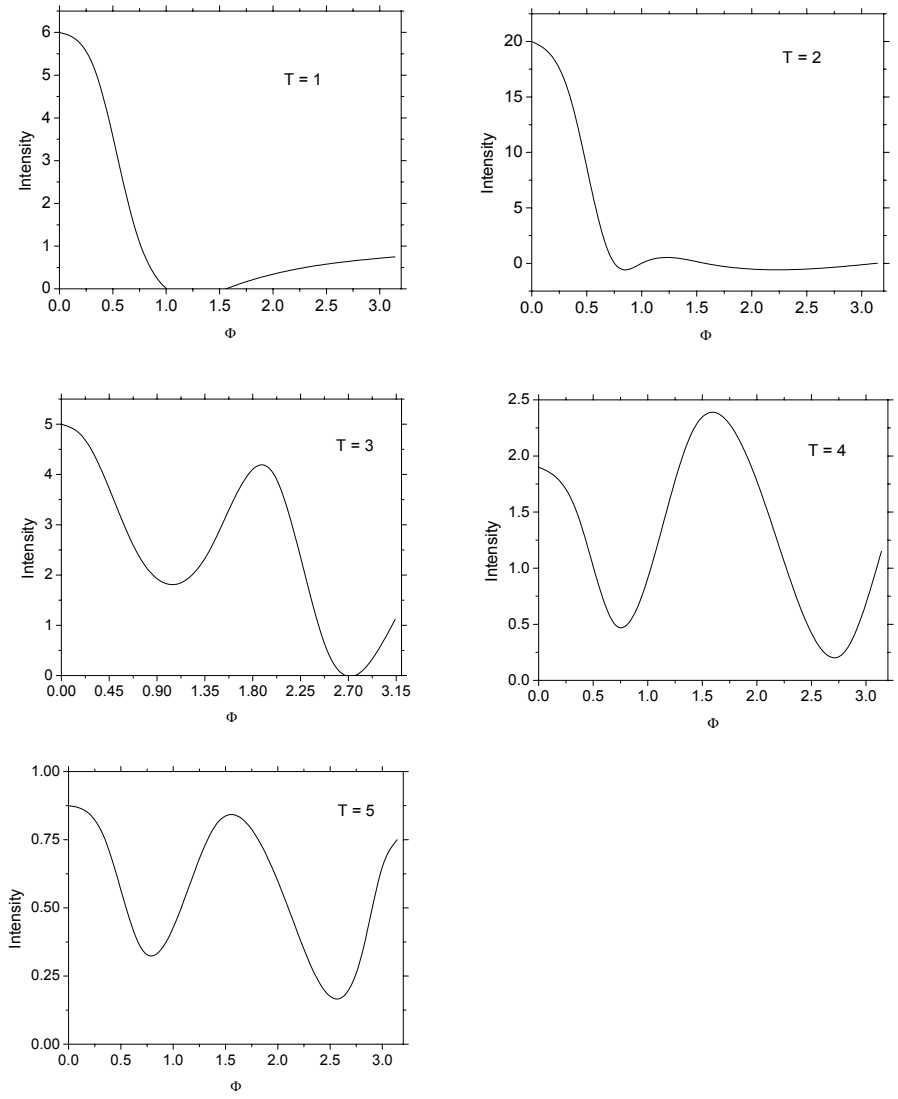

Mel'nikov, Haus, and Aitchison, Fig. 1 of 5

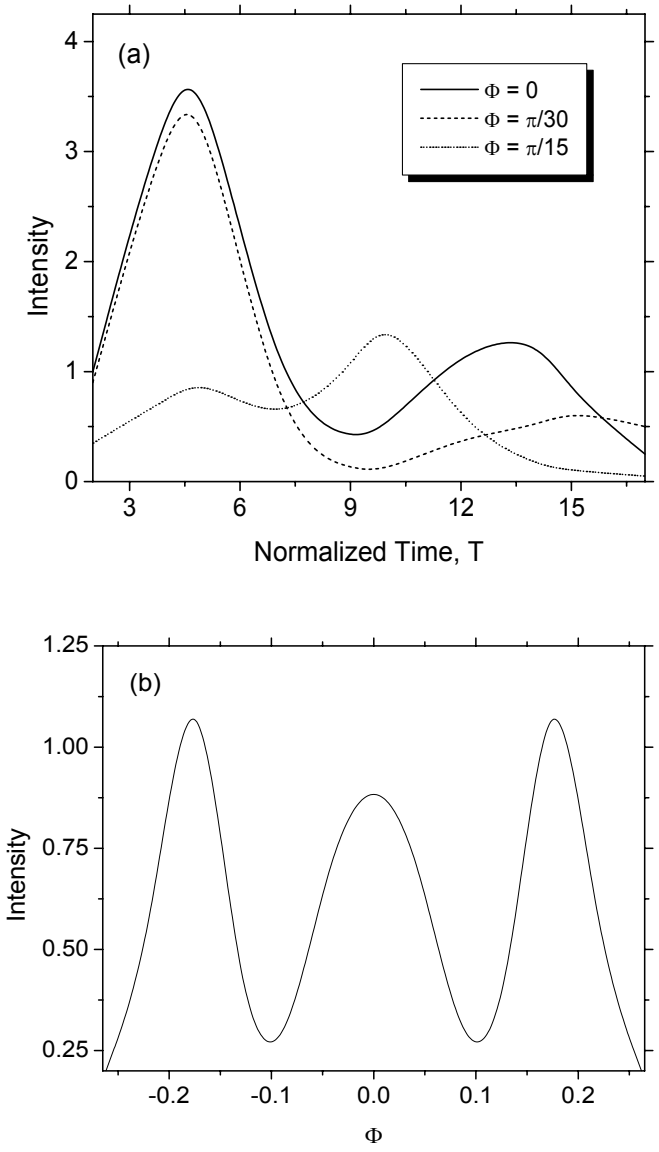

Mel'nikov, Haus, and Aitchison, Fig. 2 of 5

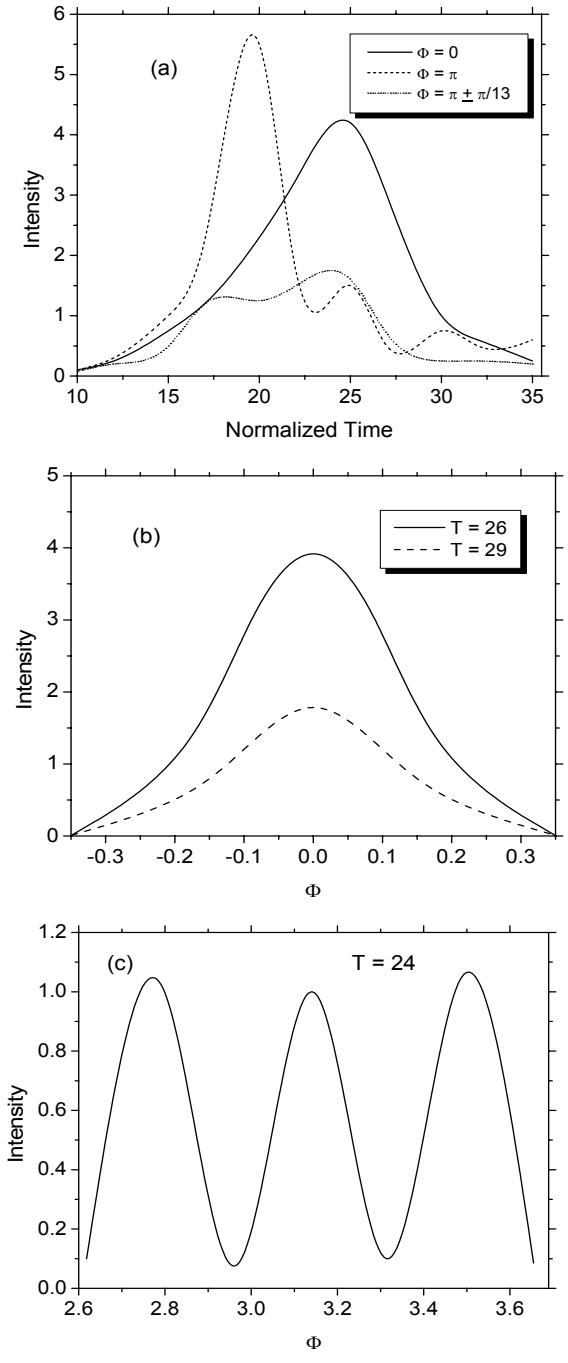

Mel'nikov, Haus, and Aitchison, Fig. 3 of 5

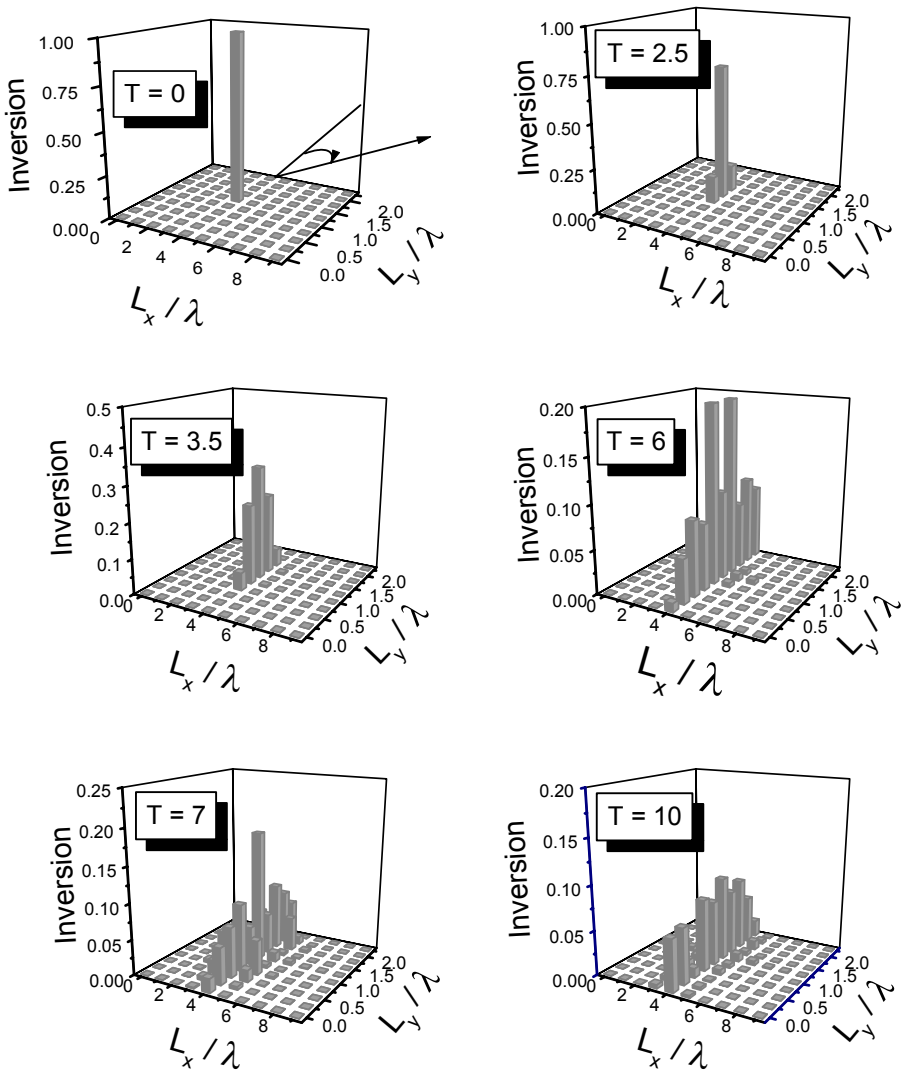

Mel'nikov, Aitchison, and Haus, Fig. 4 of 5

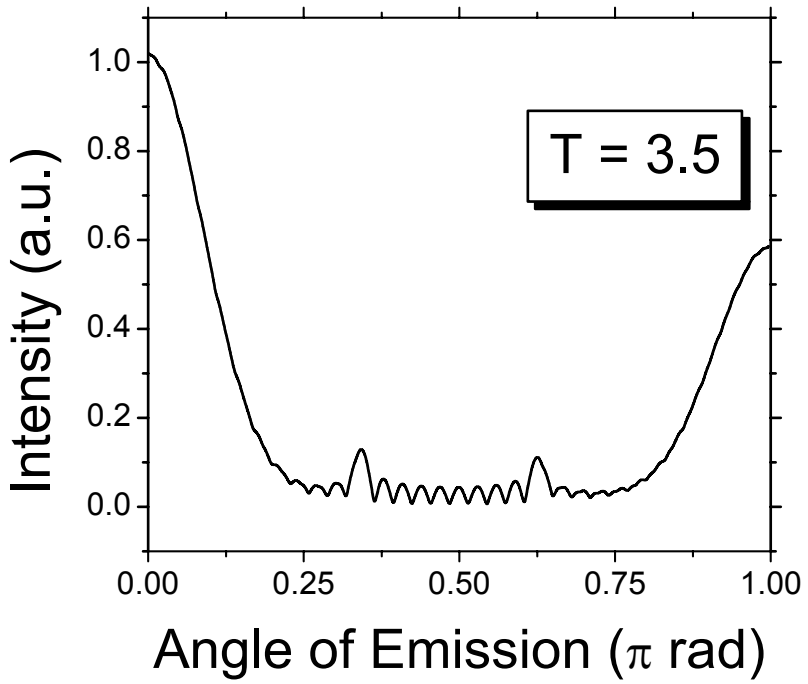

Mel'nikov, Aitchison, and Haus, Fig 5 of 5